HIGH DYNAMIC RANGE VLA OBSERVATIONS OF EIGHT CORE-DOMINATED QUASARS

R. I. KOLLGAARD,[a] J. F. C. WARDLE, AND D. H. ROBERTS
Department of Physics, Brandeis University, Waltham, Massachusetts 02254
Received 20 April 1990

ABSTRACT

The Very Large Array has been used at 5 GHz to make high dynamic range observations of eight quasars with prominent cores. All exhibit one-sided jets, and all but one show evidence of diffuse halos. The luminosity of the extended emission by itself is sufficient for these to be Fanaroff–Riley Class II radio sources. This interpretation is confirmed by the polarization of the extended structure: the inferred magnetic field is parallel to the jet axis in all cases, and in all but one instance turns to be nearly perpendicular to the jet at its outer end. We identify these latter structures as classical terminal hotspots. Both the total intensity data and especially the polarization data strongly support the notion that these quasars are similar to the classical lobe-dominated quasars, but are oriented with jet axes close to the line of sight. If this is so, then the relatively high degrees of polarization observed in the terminal hotspots appear to require that the downstream fluid velocities in the hotspots are mildly relativistic, in the range $0.2 \leqslant v/c \leqslant 0.8$. This, in turn, implies that the jets are at least moderately relativistic over their entire length.

I. INTRODUCTION

Detailed observations of the faint features around compact, core-dominated radio sources can help determine what relationship, if any, they have with larger, lobe-dominated sources. It has been suggested by Orr and Browne (1982) that flat-spectrum core-dominated quasars are simply steep-spectrum "classical lobe-dominated quasars" (hereafter referred to as CLDQs) seen at small angles to the line of sight. Beaming effects due to the relativistic velocities of the outflow, both on the milliarcsecond and arcsecond scale, may account for the morphological and spectral index differences seen between these quasars classes, although attempts to test for these effects statistically are heavily dependent on the model for the core emission (Lind and Blandford 1985). On the other hand, it is in principle possible to disprove a unified scheme if clear differences are seen in the galactic environment of two populations that are thought to be intrinsically identical, or if differences in morphology or other properties are seen that cannot be explained by changes in orientation. Some differences between the cluster environments of compact and extended sources have been found by Prestage and Peacock (1988); this argues against a unified scheme, at least for lower-luminosity sources.

A unified scheme connecting flat- and steep-spectrum quasars makes several rather general predictions concerning the extended radio features of core-dominated objects. Principally, they should have diffuse halos corresponding in morphology, spectrum, and luminosity to the lobes of CLDQs. Thus they should exhibit one-sided jets and should be "edge brightened" ["FR II," Fanaroff and Riley (1974)] with the peak emission near the outer edge of the lobe (i.e., have a bright hotspot), not "edge darkened" ("FR I"). This simple prediction may, however, be altered in sources oriented close to the line-of-sight, especially if the jets are relativistically enhanced. Small intrinsic bends can be greatly exaggerated, distorting the relationship of the jet to the terminal hotspot in the lobe. Care must also be taken in estimating the luminosity of the extended structure, if this includes jetlike features that may be significantly enhanced by beaming.

[a] Present address: Astronomy Department, Pennsylvania State University, University Park, PA 16802.

Polarization observations of the extended structure associated with core-dominated quasars are also important for establishing the connection with CLDQs, and may be less sensitive to projection and beaming effects. In general, the magnetic field in FR I sources is perpendicular to the jet, except near the core of some objects where it is parallel (Bridle and Perley 1984). In FR II sources the magnetic field is parallel to the jet over its entire length, until the terminal hotspot, where the field is more nearly perpendicular (Bridle 1986; Scheuer 1987b). These signatures are unlikely to be greatly distorted by projection or aberration.

Detailed observations of core dominated quasars have been made by, among others, Perley (1982), Browne *et al.* (1982a,b), Schilizzi and de Bruyn (1983), van Bruegel, Miley, and Heckman (1984), Pearson, Perley, and Readhead (1985), and O'Dea, Barvainis, and Challis (1988). The observed morphology of core-dominated quasars is found to be generally consistent with what one would expect if these sources are CLDQs oriented with their jet axes close to the line of sight. They are of small (projected) linear size; they often exhibit hotspots and bent jets, and where diffuse halos are detected they generally overlap the core.

Determining if the flow in the arcsecond jets of quasars is moving at relativistic velocities is important whether or not unified schemes are correct. There are several consequences of relativistic speeds which, in principle, can be used to determine the speed, although they require simplifying assumptions (Perley 1984). Beaming will increase the observed flux from an approaching component and decrease that from a receding one. An estimate of the jet speed can be made from the ratio of these fluxes if it is assumed that the components are traveling in precisely opposite directions and that they are intrinsically identical. For sources oriented close to the line-of-sight, however, even small intrinsic bends can lead to large variations in the amount of Doppler enhancement. This weakens the reliability of speed estimates based on this method. Also, numerical simulations of jets have shown that there may be a considerable backflow near the head of an advancing jet (Smith *et al.* 1985). This backflow will affect the observed brightnesses of a jet and a counter-jet, further corrupting the speed estimate.

Making use of time-of-flight effects, an estimate of the rate

 0004-6256/90/041057-16$00.90

TABLE I. Source and observing parameters.

Source (1)	Alias (2)	z (3)	α_{20}^{6} (4)	Scale[a] (5)	Epoch (6)	Array (7)	T_{obs} (h) (8)
0106 + 013	4C 01.02	2.107	+ 0.49	4.05	1986.45	A/B	0.7
0923 + 392	4C 39.25	0.699	+ 1.15	3.98	1983.93	A/B	3.8
1328 + 307	3C 286	0.849	− 0.55	4.16	1983.93	A/B	0.4
1637 + 574		0.745	+ 0.46	4.05	1983.93	A/B	2.1
1638 + 398	NRAO512	1.66	+ 0.56	4.23	1985.13	A	1.3
1642 + 690	4C 69.21	0.751	+ 0.25	4.06	1985.42	B	1.1
1928 + 738	4C 73.18	0.302	+ 0.03	2.76	1984.23	B/C	0.6
1954 + 513		1.230	+ 0.06	4.31	1985.42	B	1.6

[a] In kpc per arcsecond for $H_0 = 100$ km s^{-1} Mpc^{-1}, $q_0 = 0.5$.

of advance of the hotspots can be made by comparing the distances of the hotspots from the core on the two sides of the source (Longair and Riley 1979). This also can easily be upset by bending if the axis of the source is close to the line-of-sight, and also requires the assumption of intrinsic bilateral symmetry. If this assumption is correct, and if the differences in hotspot locations and fluxes are due only to relativistic effects, then we would expect the brighter hotspot to be located further from the core. In the list of sources analyzed by Longair and Riley this correlation is strikingly absent. This calls into question any argument based on the assumption of strict bilateral symmetry in extragalactic radio sources.

An entirely different way of estimating the speed of a terminal hotspot in an FR II source has been outlined by Flatters and Conway (1985), based on the observed degree of polarization of the hotspot. This method assumes that the magnetic field in the jet has been compressed at its terminal shock in the manner described by Laing (1980). The observed degree of polarization from the compressed "Laing sheet" depends on the orientation of the Laing sheet with respect to the observer in the frame of the emitting fluid (downstream from the hotspot). The modification of this orientation by relativistic aberration leads to an estimate of the speed. Speed estimates from this method require knowledge of the angle between the jet and the line of sight, although no assumption about the bilateral symmetry of the source is needed. It is also necessary to assume that the Laing sheet is perpendicular to the jet, but this can be checked in part from the observed polarization position angles.

Throughout we have assumed $H_0 = 100$ km^{-1} s^{-1} Mpc^{-1} and $q_0 = 0.5$, and the spectral index α is defined such that $S_\nu \propto \nu^{+\alpha}$.

II. OBSERVATIONS

Our observations were made with the Very Large Array* (VLA) while it was being used as part of a VLBI network. As such, the array configurations were not always optimal for observations of compact sources and the resulting images have a variety of resolutions and noncircular beams. Table I gives a log of the observations, the columns giving (1) the IAU source name, (2) an alias, if any, (3) the redshift (taken from Hewitt and Burbidge 1987), (4) the spectral index between $\lambda\lambda$ 6 and 20 cm, taken from Perley (1982), (5) the image scale in kpc/arcsec, (6) the epoch of observation, (7) the array configuration of the VLA, and (8) the number of hours of observing time. For all the observations a frequency of 4985.0 MHz and a bandwidth of 50 MHz were used.

Since the data were recorded as part of a phased-array VLBI experiment, the observations were made with the on-line gain corrections disabled. Thus system temperature corrections were made off-line as part of the calibration process. All subsequent data reduction was done in the usual manner for VLA data. Initial calibration and editing of the data were done on site, with the amplitude calibration being based on observations of 3C 286, using the flux-density scale of Baars *et al.* (1977). Imaging and measurement were done at Brandeis using the AIPS package of the NRAO. Fourier transforming and CLEANing of the data were performed with the task MX, from which models were derived for use with the self-calibration task ASCAL, resulting in an improved dataset for use with MX again. Two iterations of this procedure, with corrections being made only for the visibility phases, were followed by 5–8 more iterations where both phase and amplitude corrections were applied. Corrections were also made for time-independent baseline-dependent errors using the tasks BCAL1 and BCAL2. These were based on observations of 3C 84 and were applied after the first phase-only use of ASCAL.

Very high dynamic range images of the quasar 3C 345 have also been made using phased array data (Kollgaard, Wardle, and Roberts 1989) and comparison of the off-core features (which are almost certainly nonvariable) at different epochs shows that the amplitude scale of images made from such data are probably only accurate to ~15%. Similar phased array data have also been used by Walker, Benson, and Unwin (1987) to produce very high dynamic range observations of the radio source 3C 120.

Small amounts of VLA data in the normal ("interferometer") mode were recorded during times when the other telescopes of the VLBI network were making calibration observations. These data were treated independently from the phased array data, and although preliminary images were made from them, they were not incorporated in most of the images shown here. In three cases (0106 + 013, 1928 + 738, 1954 + 513), where the quantity of interferometer mode data was $\gtrsim 50\%$ of the phased array mode data, it was deemed useful to combine the two datasets after self-calibrating them separately. Because phased array observations are more vulnerable to phase jumps in the reference antenna, the interferometer data were also used to confirm the posi-

*The National Radio Astronomy Observatory is operated by Associated Universities, Inc., under cooperative agreement with the National Science Foundation.

TABLE II. Measured source parameters.

Source (1)	Component (2)	I(mJy) (3)	m (%) (4)	χ (deg) (5)
0106 + 013	core	3873	2.5	96
	jet	150	25	85
	S knot	92	5	100
0923 + 392	core	5518	0.3	165
	jet	80	30	173
	E knot	53	20	95
	halo	200	—	—
1328 + 307	core	7177	11.2	32
	jet	90	< 20	—
	W knot	35	25	85
1637 + 574	core	1708	3.8	105
	jet	25	< 20	—
	halo	85	—	—
1638 + 398	core	752	0.6	112
	jet	6	—	—
	N lobe	2	—	—
1642 + 690	core	1350	4.3	114
	S jet	100	10	86
	S knot	20	15	126
	N lobe	17	18	20
	halo	50	—	—
1928 + 738	core	2776	2.7	93
	S jet	25	15	74
	S knot	6	29	118
	N lobe	40	< 31	—
1954 + 513	core	1453	0.6	25
	N jet	90	8	70
	N lobe	15	30	75
	N knot	7	10	133
	S lobe	32	15	71

tion angles of the electric vectors in the polarized images. In no instance was a discrepancy found between images made with the two datasets.

III. RESULTS

Total intensity and polarization images of the eight sources we observed are shown in Figs. 1–8. On each image the resolution may be judged from the 50% contour of the core component. A summary of the observed properties of the more distinct features is given in Table II. This shows (1) the source name, (2) the type of component, (3) the integrated total intensity from the component, (4) the percentage polarization m of the component, and (5) the position angle χ of the electric field at the peak of polarization, without any rotation measure correction. The percentage polarization has been determined by a comparison of the peak flux densities on the total intensity and polarized images, and so, for jets, applies only to the brightest regions in total intensity. The rotation measure, when known, is stated in the discussion of each source. No corrections for Faraday rotation have been applied to the polarized images since (a) they are small in all cases (< 31 rad m^{-2}), and (b) the measured values strictly apply only to the core and not necessarily to the extended structure. A rotation measure of 30 rad m^{-2} implies a rotation of only 6° at a wavelength of 6 cm.

a) 0106+013 (4C 01.02)

No high dynamic range images of this quasar have been published. VLA observations by Perley (1982) at 5 and 1.5 GHz revealed a single secondary component 4\".4 south of the core at position angle 185°. Early VLBI observations (Preston *et al.* 1985) showed only an unresolved core. A recent 5 GHz VLBI image made by Wehrle, Cohen, and Unwin (1990) shows a ~ 1 mas double structure oriented roughly east–west. Hence there is considerable bending between milliarcsecond and arcsecond scales. Based on two epochs, the separation of the two VLBI components is increasing at $\mu = 0.2$ mas/yr, corresponding to an apparent superluminal velocity of $v/c = 8.2h^{-1}$. Thus 0106 + 013 joins the list of superluminal quasars.

Figure 1(a) shows our VLA total intensity image made from uniformly weighted data. A weak jet with a bright knot extends to the south. The jet appears to have a slight wiggle, although this may be somewhat exaggerated by uncertainties in the lowest contour. Unlike the other quasars in this study no traces of a diffuse halo were definitely seen, although these images have the lowest dynamic range of all those shown here.

Figure 1(b) shows a polarized image made with natural weighting. The rotation measure has been found to be -11 rad m^{-2} by Simard–Normandin *et al.* (1988) and -4 rad m^{-2} by Rudnick and Jones (1983). Polarized emission is seen along the entire length of the jet, although it is concentrated in two bright knots. The orientation of the **E** vectors is closely perpendicular to the direction of the jet, so the inferred magnetic field is parallel to the jet. The brightest knot is much less prominent in polarized flux than in the total intensity; its degree of polarization ($m \simeq 5\%$) is significantly less than the rest of the jet, which is about 25% polarized. The total intensity morphology of the bright knot has the appearance of a terminal hotspot, although the magnetic field of the knot remains parallel to the jet.

New higher dynamic range observations made at $\lambda\lambda$ 3.6 and 6 cm (Kollgaard, Roberts, and Wardle, in preparation) show an additional faint knot just beyond the bright knot 4\" south of the core, and in this knot the magnetic field turns to be orthogonal to the jet direction. The new images also show clearly an extended lobelike feature 2\" northeast of the core. This is visible at the lowest contour level in Fig. 1(a).

b) 0923+392 (4C 39.25)

VLBI observations of this quasar by Shaffer *et al.* (1987) have shown both superluminal and stationary components east of the core. The complex arcsecond structure has been imaged with MERLIN at 1.7 GHz (Browne *et al.* 1982a) and 408 MHz (Browne *et al.* 1982b). The 408 MHz image reveals a close triple surrounded by an amorphous halo. The core does not strongly dominate. At 1.7 GHz the diffuse halo was not observed, and a stronger core is flanked by two jetlike extensions each about 2\" long.

Figure 2(a) shows our total intensity image of 0923 + 392 at a resolution of $\sim 0\overset{\prime\prime}{.}3$. The basic triple structure seen at 408 MHz is visible, although the core is much more dominant at 5 GHz. A naturally weighted image did not show significantly more flux or further extensions in the halo. While it is difficult to separate completely the halo from the brighter jetlike extensions, subtraction of the core and the bright knot in the east (assuming that they are unresolved) leaves the halo with a contribution of about 200 mJy.

The distribution of linearly polarized emission is shown in Fig. 2(b). The rotation measure has been reported as 15 rad m^{-2} by Rudnick and Jones (1983) and 32 rad m^{-2} by Rusk (1988). The core is weakly polarized ($m \simeq 0.3\%$) and does not contribute much more polarized flux than does the bright knot at the end of the eastern jet ($m \simeq 20\%$). Down to

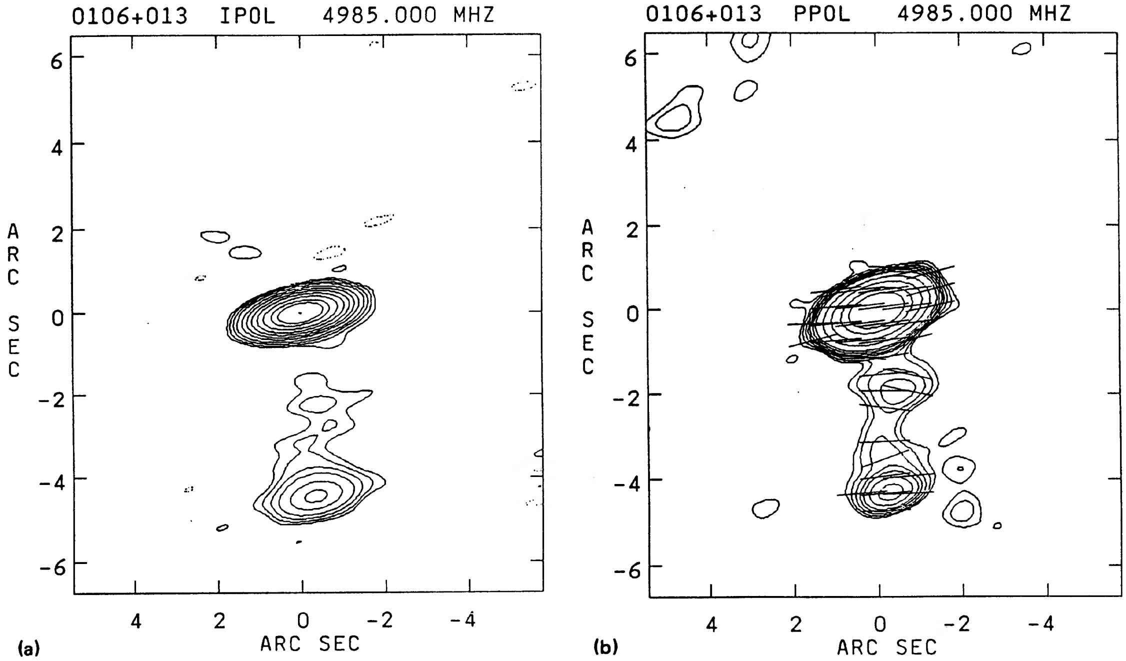

FIG. 1. 0106 + 013. (a) Total intensity distribution with levels − 0.1, − 0.05, 0.05, 0.1, 0.2, 0.4, 8, 16, 32, and 50% of the peak flux of 3.88 Jy/beam. The beam is 1″1 × 0″4 at 102°. (b) Linear polarization intensity with electric field vectors indicated by the sticks, and levels 1.00, 1.25, 1.6, 2.0, 2.4, 3.1, 4, 8, 16, 32, and 50% of the peak flux of 98 mJy/beam. The beam is 1″4 × 0″8 at 107°.

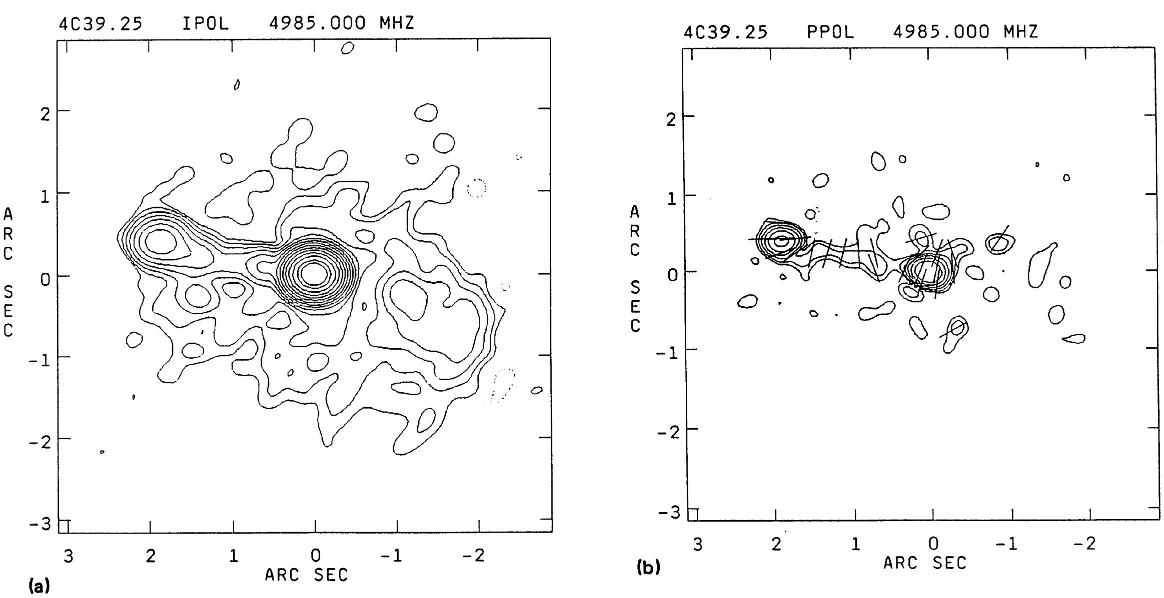

FIG. 2. 0923 + 392. (a) Total intensity distribution with levels − 0.016, − 0.008, 0.008, 0.016, 0.032, 0.063, 0.125, 0.25, 0.5, 1, 2, 4, 8, 16, 32, and 50% of the peak flux of 5.524 Jy/beam. The beam is 0″32 × 0″27 at 87°. (b) Linear polarization intensity with electric field vectors indicated by the sticks, and levels 6, 9, 14, 21, 32, and 50% of the peak flux of 17.8 mJy/beam. The beam is 0″32 × 0″27 at 87°.

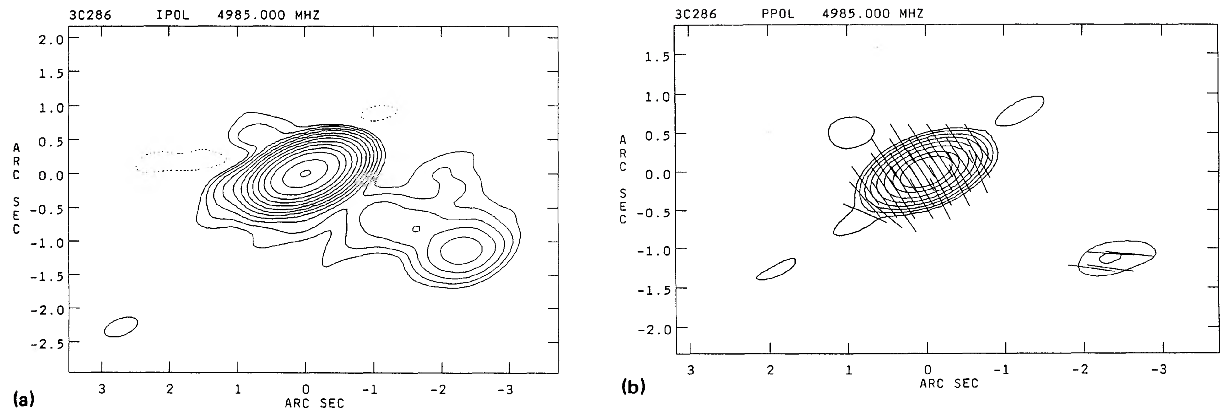

FIG. 3. 1328 + 307. (a) Total intensity distribution with levels − 0.020, 0.020, 0.030, 0.045, 0.070, 0.10, 0.16, 0.32, 0.63, 1.5, 3, 6, 12, 24, and 50% of the peak flux of 7.19 Jy/beam. The beam is 0″69×0″35 at 111°. (b) Linearly polarized intensity with electric field vectors indicated by the sticks, and levels 0.5, 1, 2, 4, 8, 16, 32, and 50% of the peak flux of 806 mJy/beam. The beam is 1″4×0″8 at 111°.

a level of about 900 μJy/beam, no polarized emission is seen west of the core. The eastern jet, however, does contribute over its entire length, the magnetic field being oriented nearly parallel with the jet, except at the terminal knot, where it is perpendicular to the jet. The bending on the western side of the terminal knot is exaggerated by the partial cancellation of some of the polarized emission due to differences in field orientations. The jet contributes about 25 mJy of the total of 50 mJy seen in this image.

c) 1328+307 (3C 286)

Unlike the other sources in this work, 1328 + 307 has a comparatively steep spectrum (Baars *et al.* 1977; $\alpha = -0.55$ between 5 and 1.5 GHz; Perley 1982). It is also nonvariable (it is a flux and polarization standard at the VLA). Total intensity images have been made by Pearson, Perley, and Readhead (1985) using the VLA at 5 GHz. They found a single secondary 2″6 from the core at position angle 245°. The secondary was elongated in the direction of the core, although it was not clear if it was connected via a jet or bridge. Total intensity and polarization images showing the same features have also been made by van Bruegel, Miley, and Heckman (1984) at 5 and 15 GHz with the VLA. VLBI observations (Kus *et al.* 1988) show an initially straight jet which bends toward the arcsecond features.

Our total intensity image is shown in Fig. 3(a). The main secondary, 2″6 southwest of the core, has a jetlike extension that almost reaches back to the core. Traces of a diffuse halo seem to be surrounding the jet. The core is elongated somewhat to the east (along position angle 105°), although, unfortunately, the elliptical resolution of our observations prevents this from being adequately resolved. This feature is consistent with the small eastern extensions seen in previous images, and may represent a counter-jet. Our image is based on only a single snapshot, and suffers from poor $u-v$ coverage. A much higher dynamic range image has been published recently by Hines, Owen, and Eilek (1989). This confirms the main features in our image, but the faint emission to the northeast of the core and surrounding the jet may not be real.

Figure 3(b) shows our polarized image. The rotation measure is 0 rad m^{-2} (Rudnick and Jones 1983; VLA calibrator manual). As in the image by van Bruegel, Miley, and Heckman (1984), only the core and main secondary were definitely detected in polarization. The fractional polarization of the jet is less than 20%. 3C 286 is an extremely unusual source in that its core is so strongly polarized. We see here that the inferred magnetic field direction in the core is nearly orthogonal to both the milliarcsecond and the arcsecond scale jets. (Note that both the degree of polarization and the spectrum of the core indicate that it is optically thin.) This is also unusual among quasars with appreciably polarized cores (Rusk 1988; Roberts and Wardle 1990).

d) 1637+574

While no high dynamic range observations have been published of this quasar, there have been indications of asymmetric, diffuse features about the bright core. Owen, Porcas, and Neff (1978), using the Greenbank Interferometer at 2.7 GHz, reported a relatively prominent secondary component, with a peak brightness 14% that of the core, 8″ from the core at position angle 240°. Kapahi (1981) observed this source with the WSRT at 5 GHz and did not detect this feature, but he noted that the core was elongated by 2″ along position angle 216°. Perley (1982), using the VLA, reported diffuse emission 6″ from the core to the north and northwest, as well as structures less than 0″2 in size along position angle 220°. VLBI observations (Pearson and Readhead 1988) show a possible faint extension from the core along position angle 242°, although their data are also consistent with a single unresolved component.

Figure 4(a) shows our highest resolution image, made with uniformly weighted data. A faint jetlike extension, approximately 1″3 long, extends to the southwest, curving slightly westward. Traces of larger-scale structure are visible around the core and in the northwest. This diffuse emission is better represented in the image shown as Fig. 4(b), made with heavily tapered, naturally weighted data. While the general features of the extended emission are probably cor-

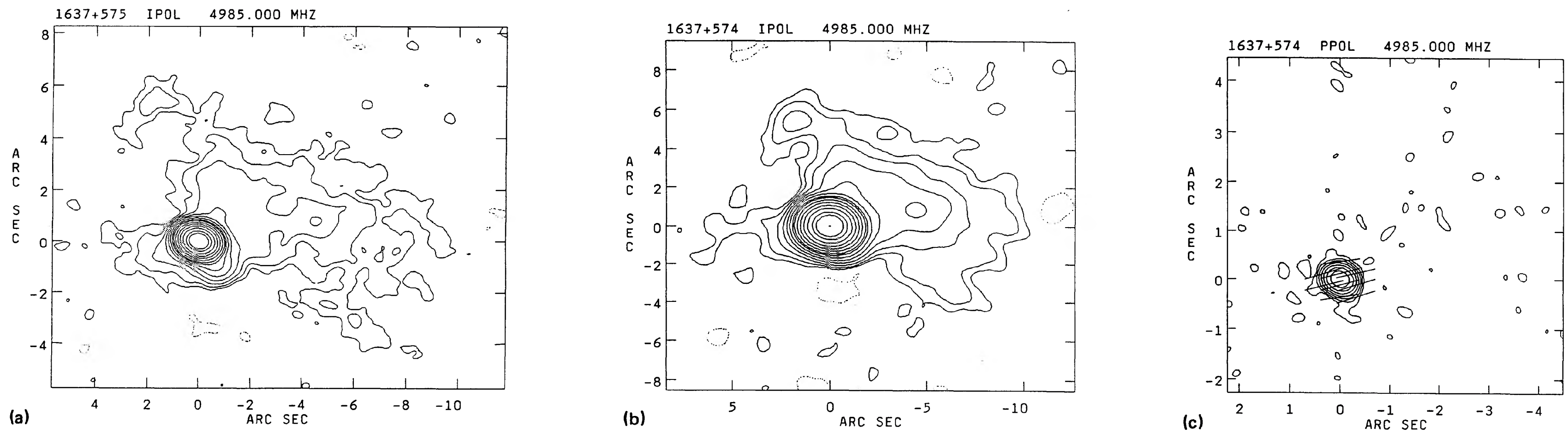

FIG. 4. 1637 + 574. (a) Total intensity distribution with levels −0.030, −0.015, 0.015, 0.03, 0.06, 0.1, 0.2, 0.4, 1, 2, 4, 8, 16, 32, and 50% of the peak flux of 1.71 Jy/beam. The beam is 0″.45×0″.37 at 64°. (b) Total intensity distribution with levels −0.02, −0.01, 0.01, 0.02, 0.04, 0.08, 0.16, 0.32, 0.64, 1, 2, 4, 8, 16, 32, and 50% of the peak flux of 1.72 Jy/beam. The beam is 1″.4×1″.1 at 83°. (c) Linearly polarized intensity with electric field vectors indicated by the sticks, and levels 0.75, 1.5, 3, 6, 12, 24, and 50% of the peak flux of 65 mJy/beam. The beam is 0″.39×0″.32 at 66°.

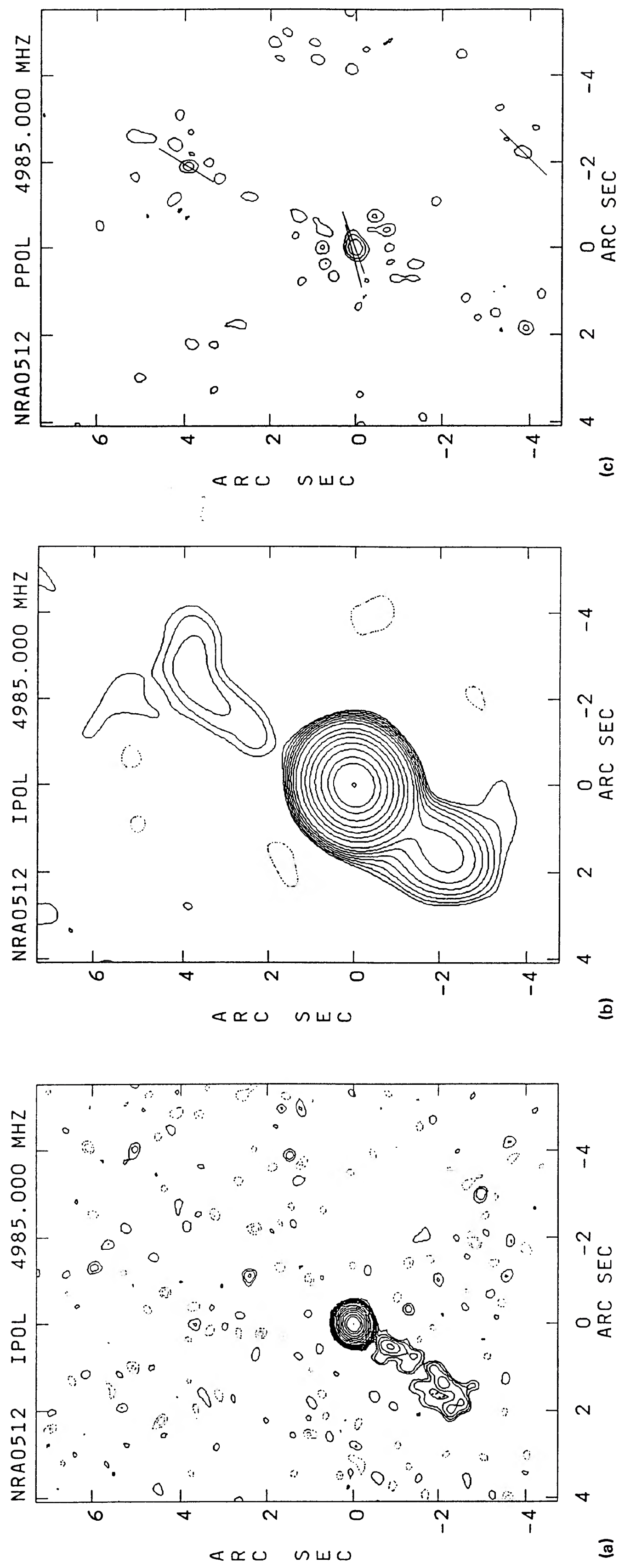

FIG. 5. 1638 + 398. (a) Total intensity distribution with levels −0.030, −0.020, 0.020, 0.030, 0.045, 0.068, 0.010, 0.15, 0.23, 0.4, 1, 2, 4, 8, 16, 32, and 50% of the peak flux of 7.52 Jy/beam. The beam is 0″34×0″31 at 106°. (b) Total intensity distribution with levels −0.030, −0.020, 0.020, 0.030, 0.045, 0.068, 0.10, 0.15, 0.23, 0.40, 1, 2, 4, 8, 16, 32, and 50% of the peak flux of 7.52 Jy/beam. The beam is 1″04×0″95 at 119°. (c) Linearly polarized intensity with electric field vectors indicated by the sticks, levels 12, 24, and 50% of the peak flux of 4.5 mJy/beam. The beam is 0″34×0″31 at 106°.

rect, the size scale is near the upper limit of accessibility to the VLA in the A configuration, and some details may not be reliable.

The polarized image [Fig. 4(c)] shows no definite polarization features outside the core, down to a limit of about 600 μJy/beam, although the core on this image is slightly extended along position angle 202°, which is near that of the VLBI jet.

e) 1638+398 (NRAO 512)

No high dynamic range arcsecond observations have been reported previously for this quasar. VLBI observations (Bartel *et al.* 1986; Brown, Roberts, and Wardle, in preparation) show only a barely resolved core with very low linear polarization.

We find emission on both sides of the core, and a morphologically complex jet. Figure 5(a) shows our highest-resolution total intensity image, made with uniformly weighted data. The jet is composed of several knots and is surrounded by a diffuse halo that may be a lobe. About two thirds of the total intensity emission from the jet is from the "detached" southernmost region.

Figure 5(b) shows a heavily tapered, naturally weighted image, where the diffuse northern emission is better represented. The amorphous halo around the jet is also more easily visible. The northern emission now has the appearance of a jetlike extension with a sharp curve at the end, somewhat similar to the morphology of the southern jet in Fig. 5(a). It is not clear if the northeastern extension of the northern lobe is real.

The polarized image in Fig. 5(c) shows no evidence of anything other than the core brighter at a level of 500 μJy/beam. Since this is not much less than the brighter off-core features seen on the total intensity images no useful limits can be placed on their degree of polarization.

f) 1642+690 (4C 69.21)

Total intensity images have been made of this quasar at a variety of frequencies and resolutions. VLBI observations (Pearson *et al.* 1986) have shown at least one superluminal component extending, with the rest of the VLBI jet, along position angle ~195°. MERLIN images made at 408 MHz (Browne *et al.* 1982b) show a slightly curving, 4."5 long jet south of the core, and a fainter lobe 6" to the north. Browne (1987) has presented a 1.5 GHz VLA image that shows these basic features as well as a large, amorphous halo roughly centered on the core. MERLIN images at 1.7 GHz (Pearson *et al.* 1986) show that the southern jet is composed of at least four bright components. Polarization images at 5 GHz (O'Dea, Barvainis, and Challis 1988) show that the jet is polarized most strongly in two bright knots. This quasar is morphologically similar to 1928 + 738, which also has a curving jet, a diffuse counter lobe, and superluminal VLBI components in the core.

Figure 6(a) shows the total intensity image we derived with uniformly weighted data. The basic morphology is the same as that seen in the 408 MHz image, although our northern lobe is somewhat larger. Traces of a faint halo are seen about the southern jet. A naturally weighted image (not shown) reveals a halo surrounding both the jet and the

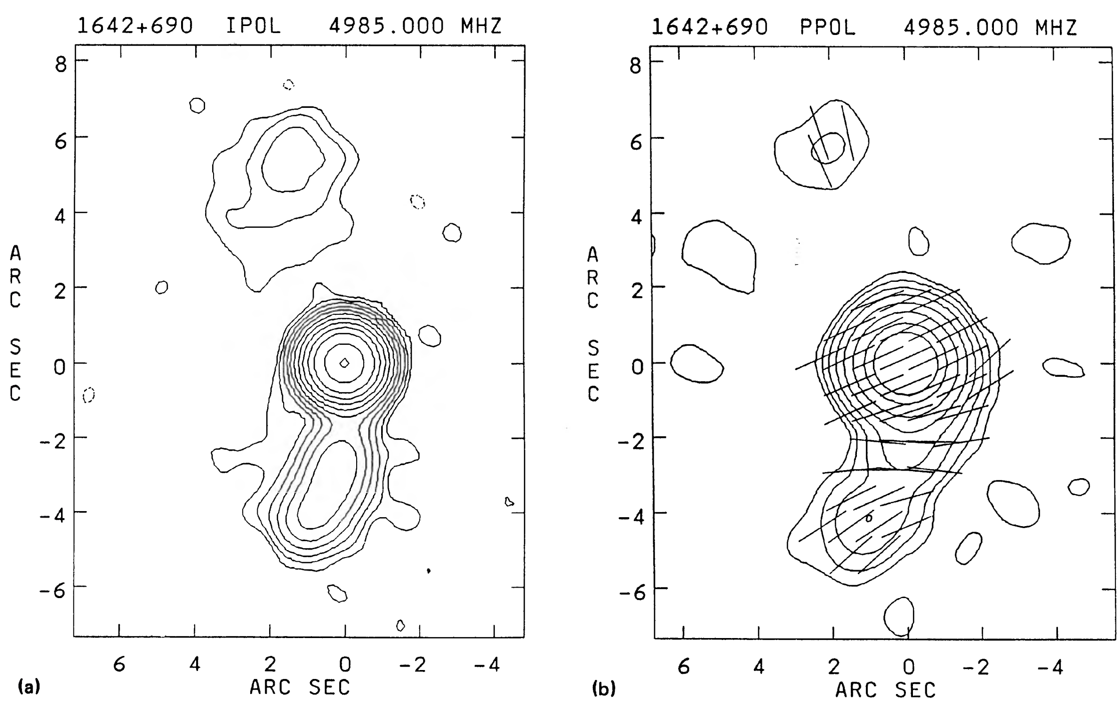

FIG. 6. 1642 + 690. (a) Total intensity distribution with levels − 0.08, − 0.04, 0.04, 0.08, 0.16, 0.32, 0.63, 1.25, 2.5, 5, 10, 20, and 50% of the peak flux of 1.35 Jy/beam. The beam is 1."05 × 1."03 at 79°. (b) Linearly polarized intensity with electric field vectors indicated by the sticks, and levels 0.5, 1, 2, 4, 8, 16, 32, and 50% of the peak flux of 59 mJy/beam. The beam is 1."72 × 1."65 at 96°.

northern lobe, as well as slight extension west of the core. Thus the halo is slightly more asymmetric at 5 GHz than at 1.5 GHz.

The distribution of linearly polarized emission is shown in Fig. 6(b). This image is made with naturally weighted data. The rotation measure is -9 rad m^{-2} (Rusk 1988). A higher-resolution image (not shown), using uniformly weighted data, confirms the features seen by O'Dea, Barvainis, and Challis (1988), and shows that in addition to the core, there are at least two bright polarized knots. These polarized knots correspond to the beginning and end of the bright portion of the jet. The magnetic fields are aligned parallel to the direction of the outflow, except at the terminal knot where the field is perpendicular. In the north Fig. 6(b) also shows a knot of polarized emission with a magnetic field perpendicular to the direction of the core. The polarized intensity peak is located about 1″ further from the core than the total intensity peak.

g) 1928+738 (4C 73.18)

High dynamic range total intensity images of this quasar have been made at several frequencies and resolutions, although no arcsecond polarization features outside the core have previously been reported. VLBI observations (Eckart *et al.* 1985) have detected superluminal motion in at least five components in a complex 15-mas-long jet. High dynamic range total intensity observations made at 1.5 GHz with the VLA and at 610 MHz with the WSRT have been presented by Johnston *et al.* (1987) and Simon *et al.* (1987). At 1.5 GHz a series of at least four bright components extend 18″ to the south, gradually bending to the east. In the north there is one bright knot and a large patch of diffuse emission about 10″ from the core. At 610 MHz the bright core is surrounded by a weak double with slightly overlapping lobes. Rusk and Rusk (1986) also show these features in VLA images made at 1.7 and 5 GHz. This quasar is morphologically similar to 1642 + 690, which also has a superluminal component in its core.

A naturally weighted total intensity image is shown in Fig. 7(a). The jets and amorphous northern lobe are clearly seen, and the details are consistent with the lower resolution 1.5 GHz image by Johnston *et al.* (1987) and the 1.7 GHz image by Rusk and Rusk (1986). We do not see the large diffuse halo surrounding the entire source seen by the latter, although this is not unexpected at our frequency and resolution. A highly tapered, naturally weighted image did show a low surface brightness extension southwest of the core, but no other indications of the diffuse halo.

Figure 7(b) shows the polarized image, which was made with naturally weighted data. The rotation measure is 30 rad m^{-2} (Rusk 1988). In addition to the core, definite polarized emission is seen only from the two brightest knots of the southern jet. Based on this, the magnetic field is parallel with the jet as it curves eastward, until the terminal knot where it is nearly perpendicular. No polarization brighter than 600 μJy/beam was detected north of the core, even though the knot 7″ north of the core is of comparable brightness to the knots in the jet.

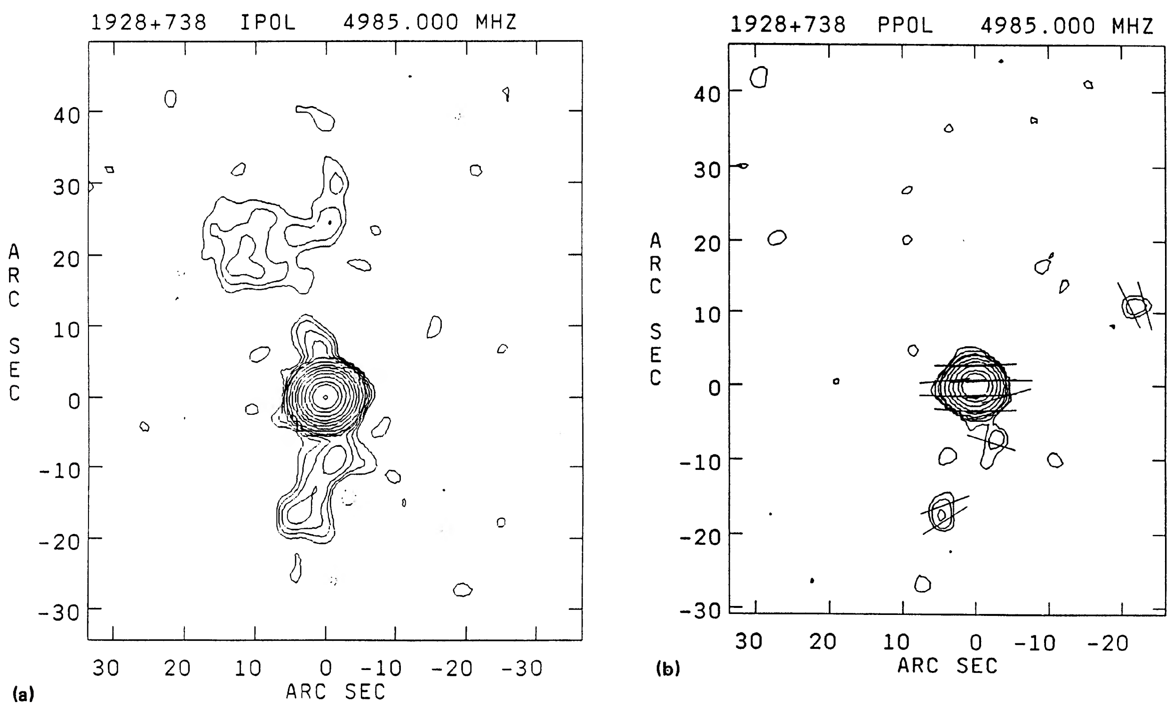

FIG. 7. 1928 + 738. (a) Total intensity distribution with levels -0.06, -0.04, 0.04, 0.06, 0.09, 0.14, 0.2, 0.4, 1, 2, 4, 8, 16, 32, and 50% of the peak flux of 2.79 Jy/beam. The beam is 3″.6×3″.4 at 102°. (b) Linearly polarized intensity with electric field vectors indicated by the sticks, and levels 0.75, 1.0, 1.5, 2, 4, 8, 16, 32, and 50% of the peak flux of 76 mJy/beam. The beam is 3″.6×3″.4 at 99°.

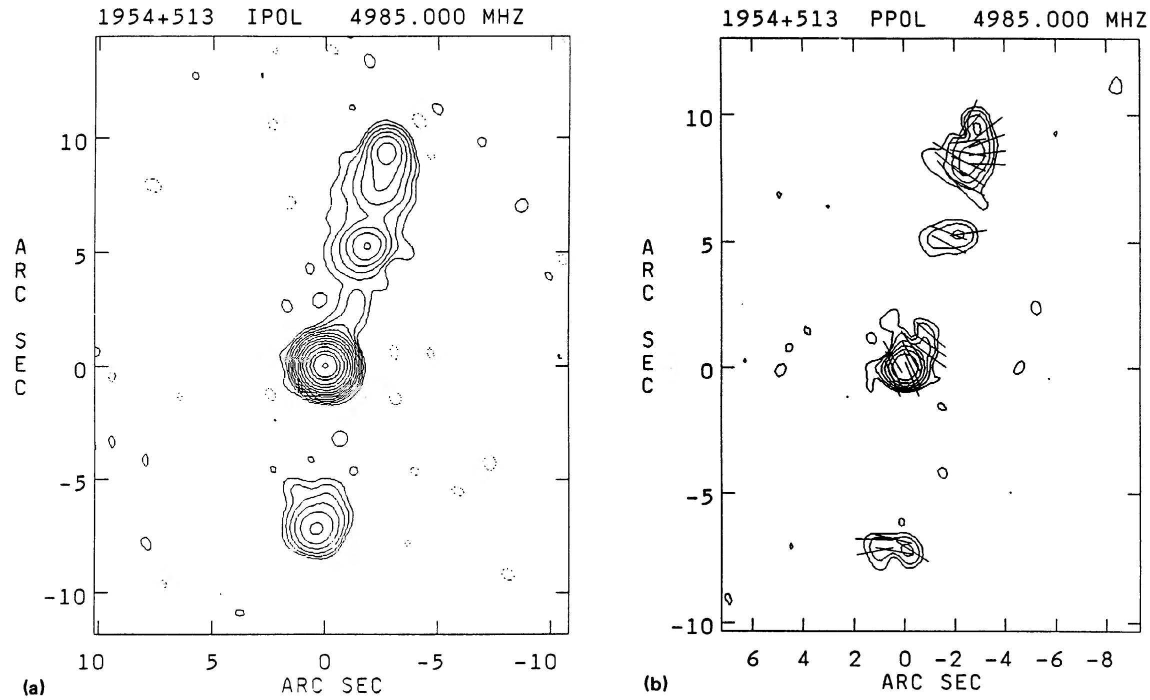

FIG. 8. 1954 + 513. (a) Total intensity distribution with levels − 0.063, − 0.032, 0.032, 0.063, 0.125, 0.25, 0.5, 1, 2, 4, 8, 16, 32, and 50% of the peak flux of 1.46 Jy/beam. The beam is 1".02 × 0".99 at 56°. (b) Linearly polarized intensity with electric field vectors indicated by the sticks, and levels 6, 9, 14, 21, 32, and 50% of the peak flux of 8.4 mJy/beam. The beam is 1".03 × 0".99 at 56°.

h) 1954+513

No high dynamic range arcsecond resolution image of this quasar has previously been published. VLBI observations (Pearson and Readhead 1988) show a faint extension from the core along position angle 36°. On the arcsecond scale, Perley (1982) reports a classical triple structure aligned along position angle 350°; this was seen at 1.5 GHz but not at 5 GHz.

Figure 8(a) shows the total intensity image made with uniformly weighted data. A 10" jet to the north connects with the core, although it is somewhat fainter along the innermost segment. The knot at the end is elongated and may consist of two bright components that are not well separated at this resolution. This knot, the knot 5".5 north of the core, and the peak of the inner jet component (3" from the core) lie on a line at position angle 348° that fails to intersect the core by about 1". Thus there must be pronounced bending of the northern jet at a distance between 1" and 3" from the core. A halo surrounds the bright knots of the northern jet, and the total flux density north of the core is ~90 mJy. Any connection between the southern component and the core must have a peak flux density of $\lesssim 500$ μJy/beam. A naturally weighted image (not shown) shows that the southern component is slightly elongated in the direction of the core, but there is no evidence of a southern jet.

The distribution of linear polarization is shown in Fig. 8(b). The core and all of the brightest knots show definite polarized flux. The knot at the end of the northern jet consists of two components that correspond to the total intensity peak 9".7 from the core and the slight extension 1" south of this. The southern knot shows two closely spaced peaks that are positioned symmetrically about the total intensity peak. The magnetic fields are everywhere oriented roughly parallel to the direction of the jet, except in the core and at the tip of the northern jet, where the inferred field directions swings by ~90°.

IV. DISCUSSION

The quasars in this study were chosen with no significant bias other than to have bright, compact cores to ensure good VLBI observations. Five are part of the complete, flux-limited sample of Pearson and Readhead (1988). Many other core-dominated quasars have also been observed by us, but those VLBI sessions took place with VLA in configuarations C or D, which are generally too small to resolve the extended structure. All the quasars observed with the A or B array, however, did show features outside the core.

We will first consider whether these quasars are either FR I or FR II class objects, based on both the total intensity and polarized properties of the jets and lobes. We will argue that the change in the position angle of polarization at the end of the jets, observed in six sources, reveals classical terminal hotspots as seen in CLDQs. We will then place lower limits on the speed of the shocked fluid in the terminal hotspots by treating the hotspots as Laing sheets. In this discussion (and in Tables III and IV) we shall include our observations of 3C 345 (Kollgaard, Wardle and Roberts 1989), which is also a member of the Pearson–Readhead sample.

TABLE III. Properties of the extended emission.

Source (1)	$\log_{10} P_{\rm extended}$ (W Hz^{-1}) (2)	R (3)	LAS (kpc) (4)	VLA P.A. (deg) (5)	VLBI P.A. (deg) (6)	VLBI $\beta_{\rm app}$ (7)
0106 + 013	26.6	8	18	185	—	
0923 + 392	26.0	12	17	77	97	3.5
1328 + 307	25.7	17	15	244	222	
1637 + 574	25.6	11	45	216	242	
1638 + 398	25.3	23	42	149	—	
1642 + 690	25.7	6	41	170	195	7.9
1928 + 738	25.0	21	140	170	166	7.0
1954 + 513	26.1	5	77	344	36	

a) The Luminosity and Morphology of the Extended Emission

All eight of the quasars observed in this study show jetlike features, and diffuse halos or lobelike structures. Table III summarizes the properties of the extended features of all of the sources (plus 3C 345); the columns give (1) the source name, (2) the log of the total power from the extended emission, (3) the ratio of the core flux to that of the extended emission. In columns (2) and (3) the data are extrapolated to an emitted frequency of 5 GHz. The flux density of the extended emission was found by subtracting the core flux density from the sum of all the clean components in the image, and therefore includes jets and hotspots. A spectral index of $\alpha = -0.75$ was assumed for the extended emission, and the spectral indices for the cores were taken from Table I. Column (4) gives the total (projected) linear size, (5) the position angle of the arcsecond scale jet with respect to the core, (6) the position angle of any milliarcsecond structure as determined by VLBI observations, and, for those sources that exhibit superluminal motion in their cores, (7) lists the apparent speed of the superluminal components.

Fanaroff and Riley (1974) showed that there is a sharp division in the 178 MHz luminosity between FR I and FR II class sources at $10^{25.8}$ W Hz^{-1}. Although they considered the total power observed, the contribution from cores and jets at 178 MHz is small, and we may extrapolate this power to 5 GHz and compare it to the power of the extended features of our eight quasars. For a spectral index of $\alpha = -0.7$, the 5 GHz Fanaroff–Riley division is $10^{24.8}$ W Hz^{-1}; for $\alpha = -1.0$, it is $10^{24.3}$ W Hz^{-1}. For all eight sources the total extended emission has a luminosity in excess of the FR limit. However, since it is likely that the arcsecond jets (and perhaps also the hotspots) are Doppler enhanced to some extent, it is more proper to use the intrinsic power of the diffuse lobe and halo emission alone, where this is possible. These are listed in column (2) of Table IV, where we have used a spectral index of $\alpha = -1.0$, which is more appropriate to diffuse features. In all cases with detectable diffuse emission, these powers are still above the corresponding Fanaroff–Riley division of $10^{24.3}$ W Hz^{-1}, even though our high-resolution images are not very sensitive to regions of low surface brightness, and it is likely that we have underestimated their flux density.

Significant luminosity in diffuse emission is a necessary but not a sufficient condition for identifying these sources as CLDQ sources seen at a small angle to the source axis. Here we briefly consider the morphology of the total intensity structure. Similar discussions have been given by, for example, Perley, Fomalont, and Johnston (1980, 1982), and O'Dea, Barvainis, and Challis (1988).

The appearance of an FR II source, when seen nearly end-on, depends on both projection effects (which exaggerate small deviations from linearity) and Doppler boosting

TABLE IV. Fanaroff–Riley characteristics.

Source (1)	$\log_{10} P_{\rm diffuse}$ (W Hz^{-1}) (2)	Halo (3)	Counter lobe (4)	Jet sidedness (5)	Polarization angle jet (deg) (6)	Polarization angle hotspot (deg) (7)
0106 + 013	25.3[a]	?	yes[a]	1	80	15[a]
0923 + 392	26.2	yes	yes	1	84	17
1328 + 307	—	?	?	2?	—	21
1637 + 574	25.8	yes	?	1	—	—
1638 + 398	25.0	?	yes	1	—	—
3C 345	26.0	yes	yes	1	55	20
1642 + 690	25.7	yes	yes	1	84	26
1928 + 738	24.7	?	yes	2?	84	10
1954 + 513	25.9	?	yes	1	86	34

[a] Based on new observations (see text).

(which changes the relative brightness of features). In the original discussion by Fanaroff and Riley, FR II sources have (by definition) their brightest off-core emission near the outer edges of the extended lobes. These are the "hotspots," thought to be strong shocks where the jets interact with the ambient medium (e.g., Meisenheimer *et al.* 1989). If the jets are Doppler enhanced (see Scheuer 1987a for a review of the evidence for this), then emission from the hotspots must be less so. Seen from a small angle to the source axis, a classical hotspot may be far less prominent than other regions in the jet. This appears to be the case in 3C 273 (Flatters and Conway 1985). Thus this defining morphological characteristic is not necessarily applicable here. We will show in the next section how the polarization data can help reveal the presence of classical hotspots.

In a unified scheme, features that we *would* expect to see in our images include one-sided jets and evidence for extended structure (lobes) on both sides of the core. The first feature must be the case since all jets in lobe-dominated quasars are one-sided (Bridle and Perley 1984; Bridle 1986). If the one-sidedness is due to Doppler favoritism, then this is enhanced when viewed at small angles to the source axis. The sidedness of the jets we observed is listed in Table IV, column (3). Seven of the nine sources show prominent jets on only one side of the core. The possible exceptions are 1928 + 738, which shows a bright jet to the south of its core, and a short feature to the north that has the appearance of a counterjet, and 3C 286, which shows a similar spurlike feature to the east of its core [most clearly seen in the higher-resolution image by Hines, Owen and Eilek (1989)]. The presence of lobelike emission on the opposite side of the core from the jet is noted in Table IV, column 4. It is clearly present in six cases. Such a feature is expected if lobe emission is not appreciably Doppler enhanced, and if the angle between the line of sight and the source axis is not so small (or the source so bent) that the "counter-lobe" is superposed on other brighter features. (Such a superposition may occur in 1637 + 574.) Numerical simulations of jets suggest that the jet fluid, after passing through the hotspot, may be swept back towards the core with significant velocity (e.g., Smith *et al.* 1985). In that case, the lobe on the jet side of the core may appear fainter than the "counter-lobe." This will be most pronounced in sources whose axes make the smallest angles to the line of sight. While it is difficult to separate jet and hotspot emission from that of a lobe, three sources (0923 + 39, 1928 + 738, and 1954 + 51) may be examples of such a backflow, and there is no clear counter example. Modest backflow velocities of $0.1c - 0.2c$ are quite sufficient to produce this effect. We note parenthetically that such modest beaming of the lobe emission further complicates the problem of choosing a sample of radio sources that is unbiased in orientation with respect to the line-of-sight (cf. Hough and Readhead 1989).

As has been argued by many authors, the total intensity properties of the extended structure around compact radio sources tend to support the now conventional picture that these sources are similar to the lobe-dominated FR II sources, but seen at a small angle to the source axis. We want to point out that the evidence is certainly not compelling in every case. In particular, three sources in Table IV do not show a counter-lobe (at our dynamic range), and two sources do show hints of possible counter jets. Since the luminosity of the extended structure we have observed already precludes their identification with FR I sources, the proper question is if they should indeed be identified with CLDQs seen at a small angle to the source axis, or if they form some third category of high-luminosity intrinsically small radio source. The polarization data shed important light on this question.

b) The Polarization of the Extended Emission

In the Orr and Browne scheme, CLDQs have distinctive polarization characteristics that should be visible in our images. First, the magnetic field should run parallel to the jet over its entire length; this signature is not affected by either projection or aberration. Second, CLDQs have terminal hotspots at the end of the jets. The projected magnetic field in the hotspots should be roughly transverse to the local jet direction, consistent with compression by a strong shock.

The polarization of various features in our sources is listed in Table II. When polarization has been detected in jetlike features, the degree of polarization is high (8%–30%). In sources whose jets are too faint for polarization to be detected, the upper limits do not preclude values in this range. Also, in each case the position angle of the **E** vectors is roughly transverse to the jet, implying a magnetic field running parallel to the jet [the angle between the **E** vectors and the local jet direction is listed in Table IV, column (6)]. This alignment of the magnetic field with the jet is what is expected in CLDQs viewed from any angle.

Of particular interest is the rotation of the angle of polarization at the end of the jets. The most striking example is 0923 + 392. Other sources that show this effect are 1328 + 307, 3C 345, 1642 + 690, 1928 + 738, and 1954 + 513. This effect was also observed in at least two additional sources observed by O'Dea, Barvainis, and Challis (1988). The angle between the **E** vectors at the tip of the jet and the local jet direction is listed in Table IV, column (6). The only counter example to this would appear to be 0106 + 013. However, as pointed out above, a higher-quality λ 6 cm image (Kollgaard, Roberts, and Wardle, in preparation) shows an additional faint knot beyond the bright knot 4″ south of the core, and in this outermost knot the **E** vectors indeed turn to be parallel to the jet direction. We identify this behavior as revealing classical hotspots as observed in lobe-dominated quasars. Indeed, this turn of the polarization **E** vectors between the end of a jet and the hotspot is perhaps the best way to distinguish between a true hotspot and a bright knot in the jet, in images of moderate resolution and dynamic range.

We conclude that the polarization properties of the extended emission in the sources we have observed add new and compelling evidence in support of the unified scheme of Orr and Browne (1982). While the polarization data do not *prove* that this unified scheme is correct in every detail, a failure to observe these signatures in the polarization, would have constituted powerful evidence against the scheme regardless of other circumstantial evidence in its favor.

c) Estimating Velocities from the Polarization of the Terminal Hotspots

High degrees of polarization have been detected in the knots of every jet (save those of 1637 + 574 and 1638 + 398 where the total intensity brightnesses are low). With the exception of 0106 + 013, the terminal hotspots in the remaining five quasars have magnetic fields nearly perpendicular to the jets, and polarizations in the range of 15%–20%.

A perpendicular field configuration is expected if the hotspot represents the "working surface" of the jet, where the field line are compressed in a strong transverse shock (Scheuer 1987b).

As an initial approximation we will treat the hotspot field configurations as being exactly perpendicular to the jets (deviations from this will be discussed below). A simple expression for the observed fractional polarization from a compressed, initially random field has been developed by Laing (1980), and extended by Hughes, Aller, and Aller (1985). In this picture the compression of an initially random magnetic field into a thin sheet (hereafter referred to as a "Laing sheet") leads to a high degree of order when viewed nearly along the plane of the sheet, making it possible for a relatively large degree of polarization to be observed from that direction. The observed degree of polarization of such a sheet is

$$m = \frac{3-3\alpha}{5-3\alpha}\,\frac{(1-k^2)\cos^2\epsilon}{2-(1-k^2)\cos^2\epsilon}, \tag{1}$$

where ϵ is the angle between the plane of the Laing sheet and the line of sight, k is the degree of compression (unit length is compressed to length k), and α is the radio spectral index (Hughes, Aller, and Aller 1985). The second term in this expression is exact only for $\alpha = -1.0$, but is an excellent approximation for other reasonable values of the spectral index.

For the quasars in this study, the jets are likely to be oriented fairly close to the line of sight, so in the absence of aberration we would expect to be viewing the Laing sheets nearly face-on, and therefore see little polarization. For $\alpha = -0.5$, $k = 0.25$ (appropriate to a nonrelativistic strong shock; Meisenheimer *et al.* 1989), and ϵ in the range 80°–60°, the expected degree of polarization is in the range 1%–9%. This is well below the values we observe. Following Flatters and Conway (1985), we attribute this apparent disagreement to modification of the angle ϵ by relativistic aberration.

For a Laing sheet moving at a speed βc in a direction normal to the plane of compression, the angle of emission ϵ in the frame of the emitting fluid, is related to the angle θ between the jet and the line of sight by the aberration formula $\cos\epsilon = D\sin\theta$, where $D = 1/\gamma(1-\beta\cos\theta)$ is the Doppler factor of the emitting fluid in the Laing sheet and the Lorentz factor is $\gamma = (1-\beta^2)^{-1/2}$. Thus the observed fractional polarization can be written

$$m = \frac{3-3\alpha}{5-3\alpha}\,\frac{D^2(1-k^2)\sin^2\theta}{2-D^2(1-k^2)\sin^2\theta}. \tag{2}$$

Equation (2) can be used to estimate the speed of a Laing sheet if some knowledge of θ is available. For the quasars in this study useful lower limits can be placed on the speeds because θ is thought to be small. Figure 9 shows the relationship of the velocity and the angle to the line-of-sight for Laing sheets with polarizations in the range observed here. For an approching Laing sheet two solutions are possible, an inside solution where aberration is so strong that the observed photons are emitted (in the frame of the Laing sheet) from the side of the Laing sheet facing the core, and an outside solution where the observed photons are emitted on the side away from the core. For the sources we observed the inside solution does not appear to be likely for an approaching Laing sheet, requiring either $\beta > 0.95$ or $\theta > 50°$. At angles greater than 90°, the inside solution represents the observed polarization from a receding Laing sheet. The overall effect of aberration is that for a receding Laing sheet we see the sheet more "face-on" and the observed degree of polarization is reduced, while for an approaching Laing sheet we see the sheet more "edge-on" and the observed degree of polarization is increased.

We note that, in principle, it may not be necessary to assume a value for the orientation of the source if a polarized hotspot is observed in the counter-lobe. Under the assump-

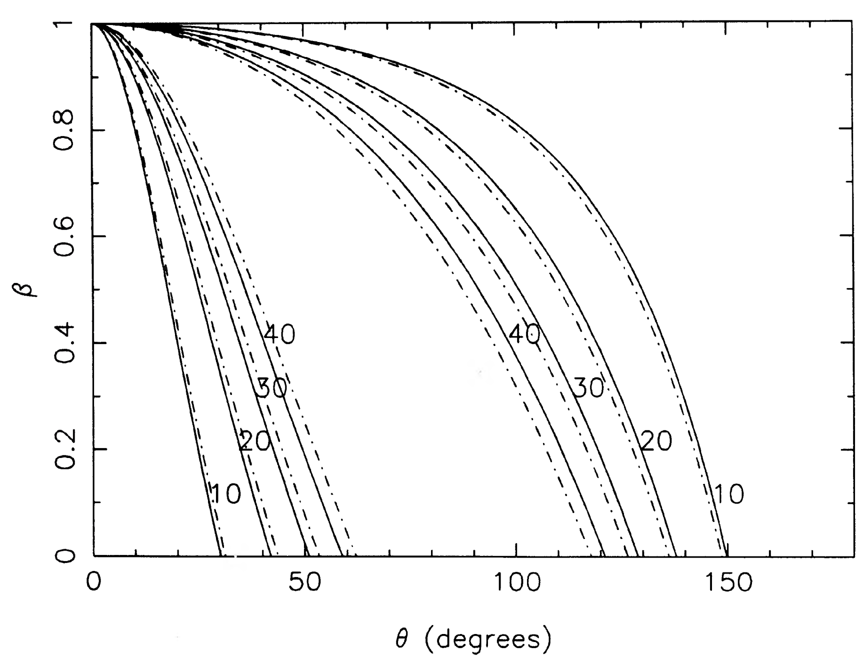

FIG. 9. Observed degree of polarization m of a Laing sheet approaching the observer with speed βc along a direction that makes an angle θ with the line of sight, as a function of β and θ. Both the "inside" and "outside" solutions are indicated for observed degrees of polarization of 10%, 20%, 30%, and 40%; the inside solution has the larger velocity for a given value of θ. Solid and broken lines are for the cases $k = 0$ and $k = 0.25$, respectively.

tion of bilateral symmetry, its fractional polarization is given by Eq. (2), with θ replaced by $\theta + 180°$. The ratio of the hotspot polarizations is

$$\frac{m_+}{m_-} = \left(\frac{D_+}{D_-}\right)^2 \frac{2 - D_-^2 (1-k^2)\sin^2\theta}{2 - D_+^2 (1-k^2)\sin^2\theta}, \tag{3}$$

where the subscripts + and − refer to the approaching and receding hotspots, respectively. Setting $k = 0$, and using the series expansions for cos and sin, we find that terms below θ^4 cancel, leading to a particularly simple expression,

$$\frac{m_+}{m_-} \sim \left(\frac{1+\beta}{1-\beta}\right)^2. \tag{4}$$

This expression is accurate to within a few percent for $\beta < 0.8$ and $\theta < 30°$, which is the range of interest here. Unfortunately, it may be difficult to use Eq. (4) in practice because the apparent polarization of the hotspot in the counter-lobe may be severely contaminated by the effects of backflow (see below). Nevertheless, this emphasizes the strong effects of aberration on the observed polarization of Laing sheets.

If we use Eq. (2) to estimate the velocity of a single hotspot, we need to know the angle θ between the Laing sheet normal and the line of sight. We do not know this for any individual quasar, but we can set reasonable limits on θ for our sources as a group. Superluminal motion has been observed in the cores of at least four of them, indicating that the nuclear jets are oriented close to the line of sight (in the range 5°–20°). Various authors have argued that the observed misalignments between the parsec and kiloparsec scale jets of core-dominated quasars are consistent with a typical intrinsic bend angle of ~10° (Rusk and Rusk 1985; Browne 1987; Rusk 1988). It seems reasonable to conclude that the orientation of the arcsecond scale jets in our sources is usually within 30° of the line of sight, with a more typical angle being perhaps 20°. It follows from Fig. 9 that *the observed degrees of polarization in the hotspots can be understood if the velocity of the emitting fluid is at least mildly relativistic—in the range 0.2–0.8 c.*

Our velocity estimate is based on a very idealized model of a terminal hotspot, so we shall discuss some obvious objections to this picture. First, we have assumed a high degree of compression of the jet fluid ($k \to 0$). In a nonrelativistic strong shock $k = 0.25$. Since this enters Eq. (2) as k^2 this error is negligible. For a weak shock the maximum degree of polarization will be smaller, and the estimated velocity will increase.

Second, the upstream (jet) fluid does not have a completely disordered magnetic field since it too exhibits appreciable polarization. It is straightforward to rework the calculation of Hughes, Aller, and Aller (1985) including a uniform magnetic field B_0 parallel to the jet axis in addition to a disordered field of magnitude B. With this addition, Eq. (1) becomes

$$m = \frac{3-3\alpha}{5-3\alpha} \frac{(1-k^2)\cos^2\epsilon - 3k^2\xi^2\cos^2\epsilon}{2-(1-k^2)\cos^2\epsilon + 3k^2\xi^2\cos^2\epsilon}, \tag{5}$$

where $\xi = B_0/B$. Noting that aberration for the upstream (jet) and downstream (hotspot) fluids will in general be different, some idea of the magnitude of B_0/B might be obtained from the observed polarization of the jet (i.e., the uncompressed fluid):

$$m_{\rm jet} = \frac{3-3\alpha}{5-3\alpha} \frac{-3\xi^2\cos^2\epsilon_{\rm jet}^2}{2+3\xi^2\cos^2\epsilon_{\rm jet}}. \tag{6}$$

For example, a jet whose degree of polarization is 20% requires $\xi \cos \epsilon_{\rm jet} = 0.52$. The result of a parallel field component in the jet is to reduce the expected polarization in the shocked fluid. Again, this increases the required aberration and hence the estimated velocity.

Third, the jet may terminate in an oblique shock, or the jet direction may turn just before the hotspot. This may be quite common in classical FR II sources (e.g., Laing 1982) and may be the cause of double hotspots. (In such a case, which hotspot we see depends critically on the Doppler enhancements.) A small bend (< 20°, say) is roughly equally likely to increase or decrease the angle between the Laing sheet normal and the line-of-sight. This has little *systematic* effect on the estimated velocities. A bend much larger than this will tend to turn the Laing sheet normal away from the line-of-sight and reduce the need for aberration. The orientation effects for an oblique shock are similar, but as the obliquity of the shock increases, the degree of compression decreases, leading to reduced polarization (Cawthorne and Cobb 1990). There is in fact a hint of such a relationship in the data (especially if combined with those of O'Dea, Barvainis, and Challis 1988), in that the more strongly polarized hotspots exhibit **E** vectors better aligned with the local jet direction. This is shown in Fig. 10. Since this possible relationship, while suggestive of oblique shocks, is based on a very small number of sources, and the observational uncertainties are large, we shall not pursue it further here.

Fourth, the picture of a hotspot as a simple Laing sheet (or Mach disk) is certainly oversimplified. The fluid flowing through the hotspot must turn around as it approaches the contact discontinuity, carrying the Laing sheet with it. It may also pass through additional conical shocks (Matthews and Scheuer 1990). Which part of such a complicated structure we actually see is then selected by several factors including orientation and beaming. These considerations may be especially important in a counter-lobe, where modest relativistic velocities in the backflow may greatly enhance these features relative to the true hotspot which may be beamed away from us. In the case of a hotspot beamed towards us, Doppler favoritism probably lessens the importance of these complications. In support of this, we note that the regions of orthogonal polarization are not noticeably displaced sideways from the tips of the jets, and that the projected magnetic field directions are indeed roughly orthogonal to the local jet direction.

In the absence of higher-resolution images it is difficult to evaluate all these effects. The basic result is that *the observed degrees of polarization in these hotspots are higher than expected for a slow Laing sheet whose normal is close to the line of sight.* The simplest interpretation is that the shocked fluid has a mildly relativistic velocity in the range 0.2–0.8 *c*. Most of the complications expected in a more realistic model will tend to *increase* this velocity estimate. We note that such speeds are entirely consistent with the recent results of Meisenheimer *et al.* (1989). They deduce postshock velocities in the range of 0.15–0.5 *c* in the frame of the shock (our velocities are in the frame of the quasar). Finally, if the hotspots are indeed shocks, then the upstream (jet) velocities must be higher (by a factor of 4 in the nonrelativistic strong shock case). This implies that the jets are at least moderately relativistic over their entire length.

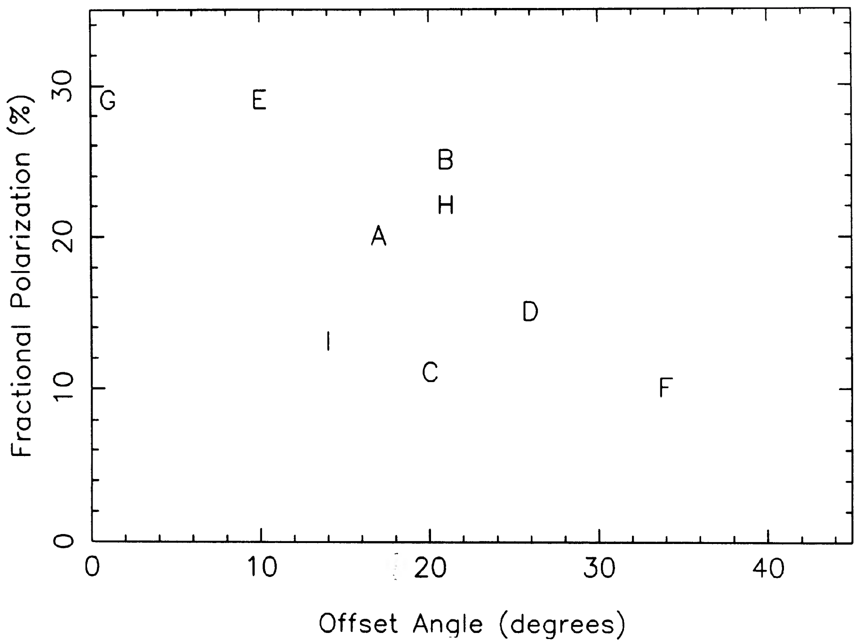

FIG. 10. The observed fractional polarization of terminal hotspots of 11 quasars vs orientation of their magnetic fields. The abscissa is the angle between the observed **E** vectors and the local jet direction. The data are from Table IV (symbols A–F), plus the sources 0605 − 085, 1510 − 089, and 1823 + 568 (symbols G–I) taken from O'Dea, Barvainis, and Challis (1988).

V. CONCLUSIONS

We have made high dynamic range 5 GHz VLA observations of the total intensity and polarization distributions of eight core-dominated quasars. The selection of these sources was essentially random, and they should fairly represent the class of core dominated quasars with VLBI-accessible cores. The quasars show arcsecond-scale structure in the form of jets, diffuse lobes, and halos. The luminosity, morphology, and polarization of the extended emission show that these are indeed Fanaroff–Riley class II radio sources, similar to the classical lobe-dominated quasars. The polarization observations are particularly useful for determining the proper classification of core dominated sources because they can be less sensitive to distortions caused by bending and relativistic beaming. The jets have inferred magnetic fields that are parallel to the jets, except at their ends, where the magnetic fields turn to be nearly perpendicular to the jets. We interpret these structures as classical terminal hotspots. The polarization results add new evidence in support of the unified scheme proposed by Orr and Browne (1982).

The terminal hotspots show large fractional polarizations and inferred magnetic fields that are nearly perpendicular to the jets. We interpret the terminal hotspots as regions of compression (Laing sheets) at the working surfaces (terminal shocks) of the jets. As core dominated quasars are likely to have jets oriented close to the line of sight, low fractional polarization is expected from such a structure unless relativistic aberration makes the working surface appear more nearly edge on. Downstream fluid velocities in the range 0.2–0.8 *c* are consistent with our observations if the quasars in this study are oriented within 30° to the line-of-sight. Uncertainties from bending in the jets and the possibility that the terminal shocks are oblique make a more precise estimate impossible. These velocities are entirely consistent with those derived by Meisenheimer *et al.* (1989) from detailed spectral observations of hotspots in other sources. The jets themselves must have higher velocities in order to form a shock and must be at least moderately relativistic over their entire length on the kiloparsec scale.

We thank Greg Lindahl for maintaining AIPS, and Leslie Brown, Tim Cawthorne, Mark Holdaway, and especially Denise Gabuzda for doing most of the on site calibration. This work was supported by the National Science Foundation under Grants Nos. AST-84-18636 and AST-89-01743 (J.F.C.W.) and Nos. AST-85-19529 and AST-88-22718 (D.H.R.).

REFERENCES

Baars, J. W. M., Genzel, R., Pauliny-Toth, I. I. K, and Witzel, A. (1977). Astron. Astrophys. **61**, 99.

Bartel, N., Herring, T. A., Ratner, M. I., Shapiro, I. I., and Corey, B. E. (1986). Nature **319**, 733.

Bridle, A. H. (1986). Can. J. Phys. **64**, 353.

Bridle, A. H., and Perley, R. A. (1984). Annu. Rev. Astron. Astrophys. **22**, 319.

Browne, I. W. A. (1987). In *Superluminal Radio Sources*, edited by J. A. Zensus and T. J. Pearson (Cambridge University, Cambridge), p. 129.

Browne, I. W. A., Clark, R. R., Moore, P. K., Muxlow, T. W. B., Wilkinson, P. N., Cohen, M. H., and Porcas, R. W. (1982a). Nature **299**, 788.

Browne, I. W. A., Orr, M. J. L., Davis, R. J. Foley, A., Muxlow, T. W. B., and Thomasson, T. (1982b). Mon. Not. R. Astron. Soc. **198**, 673.

Cawthorne, T. V., and Cobb, W. K. (1990). Astrophys. J. **350**, 536.

Eckhart, A., Witzel, A., Biermann, P., Pearson, T. J., Readhead, A. C. S., and Johnston, K. J. (1985). Astrophys. J. Lett. **296**, L23.

Fanaroff, B., and Riley, J. M. (1974). Mon. Not. R. Astron. Soc. **167**, 31p.

Flatters, C., and Conway, R. G. (1985) Nature **314**, 425.

Hewitt, A., and Burbidge, G. (1987). Astrophys. J. Suppl. **63**, 1.

Hines, D. C., Owen, F. N., and Eilek, J. A. (1989). Astrophys. J. **347**, 713.

Hough, D. H. and Readhead, A. C. S. (1989). Astron. J. **98**, 1208.

Hughes, P. A., Aller, H. D., and Aller, M. F. (1985). Astrophys. J. **298**, 301.

Johnston, K. J., Simon, R. S., Eckart, A., Biermann, P., Schalinski, C., Witzel, A., and Strom, R. G. (1987). Astrophys. J. Lett. **313**, L85.

Kaphai, V. K. (1981). Astron. Astrophys. Suppl. **43**, 381.

Kollgaard, R. I., Wardle, J. F. C., and Roberts, D. H. (1989). Astron. J. **97**, 1550.

Kus, A. J., Marecki-Trao, A., Neff, S., Van Ardenne, A., and Wilkinson, P. (1988). In *The Impact of VLBI on Astrophysics and Geophysics*, IAU Symposium No. 129, edited by M. J. Reid and J. M. Moran (Reidel, Dordrecht), p. 129.

Laing, R. A. (1980). Mon. Not. R. Astron. Soc. **193**, 439.

Laing, R. A. (1982). In *Extragalactic Radio Sources*, IAU Symposium No. 97, edited by D. S. Heeschen and C. M. Wade (Reidel, Dordrecht), p. 161.

Lind, K. R., and Blandford, R. D. (1985). Astrophys. J. **295**, 358.

Longair, M. S., and Riley, J. M. (1979). Mon. Not. R. Astron. Soc. **188**, 625.

Matthews, A. P., and Scheuer, P. A. G. (1990). Mon. Not. R. Astron. Soc. **242**, 640.

Meisenheimer, K., Röser, H.-J., Hiltner, P. R., Yates, M. G., Longair, M. S., Chini, R., and Perley, R. A. (1989). Astron. Astrophys. **219**, 63.

Moore, P. K., Browne, I. W. A., Daintree, E. J., Noble, R. G., and Walsh, D. (1981). Mon. Not. R. Astron. Soc. **197**, 325.

O'Dea, C. P., Barvainis, R., and Challis, P. (1988). Astron. J. **96**, 435.

Orr, M. J. L., and Browne, I. W. A. (1982). Mon. Not. R. Astron. Soc. **200**, 1067.

Owen, F. N., Porcas, R. W., and Neff, S. G. (1978). Astron. J. **83**, 1009.

Pearson, T. J., Barthel, P. D., Lawrence, C. R., and Readhead, A. C. S. (1986). Astrophys. J. Lett. **300**, L25.

Pearson, T. J., Perley, R. A., and Readhead, A. C. S. (1985). Astron. J. **90**, 738.

Pearson, T. J., and Readhead, A. C. S. (1988) Astrophys. J. **328**, 114.

Perley, R. A. (1982). Astron. J. **87**, 859.

Perley, R. A. (1984). In *VLBI and Compact Radio Sources*, IAU Symposium No. 110, edited by R. Fanti, K. Kellermann, and G. Setti (Reidel, Dordrecht), p. 153.

Perley, R. A., Fomalont, E. B., and Johnston, K. J. (1980). Astron. J. **85**, 649.

Perley, R. A., Fomalont, E. B., and Johnston, K. J. (1982). Astrophys. J. Lett. **255**, 193.

Prestage, R. M., and Peacock, J. A. (1988). Mon. Not. R. Astron. Soc. **230**, 131.

Preston, R. A., Morabito, J. G., Williams, J. G., Faulkner, J., Jauncey, D. L., and Nicholson, G. D. (1985). Astron. J. **90**, 1599.

Roberts, D. M., and Wardle, J. F. C. (1990). In *Parsec-Scale Radio Jets*, edited by A. Zensus and T. Pearson (Cambridge University Press, Cambridge), p. 110.

Rudnick, L., and Jones, T. W. (1983). Astron. J. **88**, 518.

Rusk, R., and Rusk, A. C. M. (1986). Can. J. Phys. **64**, 440.

Rusk, R. (1988). Ph.D. dissertation (University of Toronto).

Scheuer, P. A. G. (1987a). In *Astrophysical Jets and Their Engines*, edited by W. Kundt (Reidel, Dordrecht), p. 129.

Scheuer, P. A. G. (1987b). In *Astrophysical Jets and Their Engines*, edited by W. Kundt (Reidel, Dordrecht), p. 137.

Schilizzi, R. T., and de Bruyn, A. G. (1983). Nature **303**, 26.

Shaffer, D. B., Marscher, A. P., Marcaide, J., and Romney, J. D. (1987). Astrophys. J. Lett. **314**, L1.

Simard-Normandin, M. Kronberg, P. P., and Button, S. (1988). Astrophys. J. Suppl. **45**, 97.

Simon, R. S., Johnston, K. J., Eckart, A., Biermann, P., Schalinski, C., Witzel, A., and Strom, R. G. (1987). In *Superluminal Radio Sources*, edited by J. A. Zensus and T. J. Pearson (Cambridge University, Cambridge), p. 155.

Smith, M. D., Norman, M. L., Winkler, K. A., and Smarr, L. (1985). Mon. Not. R. Astron. Soc. **214**, 67.

van Breugel, W., Miley, G., and Heckman, T. (1984). Astron. J. **89**, 5.

Walker, R. C., Benson, J. M., and Unwin, S. C. (1987). Astrophys. J. **316**, 546.

Wardle, J. F. C., and Roberts, D. H. (1988). In *The Impact of VLBI On Astrophysics and Geophysics*, IAU Symposium No. 129, edited by M. J. Reid and J. M. Moran (Reidel, Dordrecht), p. 143.

Wehrle, A. E., Cohen, M. H., and Unwin, S. C. (1990). Astrophys. J. Lett. **351**, L1.